MATERIALS AND METHODS

Reagents. Protein and chemical reagents used (and vendors) were as follows: 8-Bromo-cAMP (8-bromo Adenosine 3′,5′-cyclic Monophosphate, β2cAMP), AKT inhibitor, G06976, LY294002, psitectorigenin and U0126: Calbiochem. PMA: Sigma. Recombinant human ICAM2-FC was produced as reported (1). Alexa fluor dye series (488, 546, 568, 594, 633, 647, 680), cascade yellow, cascade blue, allophycocyanin (APC), and R-Phycoerythrin (PE): Molecular Probes; cyanine dyes (Cy5, Cy5.5, Cy7: Amersham Life Sciences. Tandem conjugate protocols for PECy5, PECy5.5, PECy7, APCCy5.5, and APCCy7 can be found at www.drmr.com/abcon. α-CD3 (clone UCHT1) and α-CD28 (clone 28.2): BD-Pharmingen; antibodies to phosphoproteins Raf-259, Erk1/2-T202/T204, p38-T180/Y182, Jnk-T183/Y185, Akt-S473, Mek1/2-S217/S221, PKA substrates (a measure of PKA activation), PKC-S660, and Plcγ-Y783: Cell Signaling Technologies; antibodies to PIP2 and PIP3: Molecular Probes; antibodies to Erk1/2-T202/T204-phycoerythrin and PKA-S114: BD-Pharmingen. Phospho-AKT-S473 in Figure 3 was from Biosource.

Cell culture. Human peripheral blood lymphocytes were obtained by Ficoll-plaque density centrifugation (Amersham Pharmacia, Uppsala, Sweden) of whole blood from healthy donors (Stanford Blood Bank) and depleted for adherent cells. Magnetically activated cell sorting was used to negatively isolate naïve CD4+ cells (Dynal, Oslo, Norway). Human cells were maintained in RPMI-1640 supplemented with 5% human sera AB (Irvine Scientific), and 1% PSQ (1000 units penicillin supplemented with 2 mM L-glutamine). Cells were maintained at 5% CO_2 at /37^{0}C in a humidified incubator.

Flow cytometry. Intracellular and extracellular staining was performed as described (2). Intracellular probes for active kinases were made by conjugating phospho-specific antibodies to the Alexa Fluor dye series as described and used in phospho-protein staining (1, 2). Briefly, purified human CD4+ T cells were dispensed in 96 wells, and treated with chemical inhibitors for 30 min, then were treated with stimulatory agents for 15 min. Analyses were performed by direct application of fixation buffer to time-synchronized 96-wells (i.e. a single 96-well plate) maintained at 37^0C. 2% paraformaldehyde (200 uL) was added to $0.5x10^6$ cells (in 100 uL), stimulated as indicated. Fixation was performed for 30 min on pre-chilled 96-well metal holders at 4^0C. Plates were then centrifuged (1500 RPM, 5 min, 4^0C) and stained with pre-titred multi-color antibody cocktails. Cells were washed three times and analyzed. Flow cytometry data are representative of at least 3 three independent experiments. Data were collected on a custom-configured machine, a modified FACStar bench (Becton Dickenson) connected to MoFlo electronics (Cytomation, Fort Collins CO) (3). This configuration allows for 11-color analysis of samples and real-time compensation for spectral overlap (plus two channels for forward and side scatter). Data was collected using Desk software (Stanford University), compensated (intra-laser and fluorophore spectral overlap demixing) and analyzed using Flowjo software (Treestar).

siRNA inhibitions

siRNA complementary to Erk1 mRNA was purchased from Superarray Biosciences. siRNA complementary to Erk2 mRNA was purchased from Upstate Biotechnologies.

siRNA oligonucleotide (100 nM) was used in primary cell transfections using the Amaxa nucleofector systems (Amaxa Biosystems) (4).

Conditions employed. The following conditions were used for model inference: 1: (anti-CD3 and anti -CD28), 2: (anti -CD3, anti -CD28 and Intercellular Adhesion Protein-2 (ICAM-2) protein), 3: PMA (phorbol myristate acetate), 4: β2cAMP (8-bromo Adenosine 3′,5′-cyclic Monophosphate), 5: (anti -CD3, anti -CD28 and U0126), 6: (anti-CD3, anti-CD28 and G06976), 7: (anti -CD3, anti -CD28 and Psitectorigenin), 8: (anti -CD3, anti -CD28 and Akt-inhibitor), and 9: (anti -CD3, anti -CD28 and LY294002). Each condition provided 600 cells, for a total of 5400 datapoints. For the simulated western blot dataset and its single-cell equivalent, the following conditions were also used: 1 (anti -CD3, anti -CD28, ICAM2 protein and U0126), 2 (anti -CD3, anti -CD28, ICAM2 protein and G06976), 3 (anti -CD3, anti -CD28, ICAM2 protein and Akt-inhibitor), 4 (anti -CD3, anti -CD28, ICAM2 protein and Psitectorigenin,) and 5 (anti -CD3, anti -CD28, ICAM2 protein and LY294002). Equal numbers of cells (600) were selected at random from each condition, to prevent biasing the network to any particular condition.

Processing of data. Data were preprocessed as follows: Data points that fell more than three standard deviations from the mean were eliminated. Data were then discretized to three levels (low, medium or high levels of the phosphorylated protein), using an agglomerative approach that seeks to minimize loss of pairwise mutual information

among variables (5). Under conditions of chemical intervention, inhibited molecules were set to level 1 ('low'), activated molecules were set to level 3 ('high').

Simulated western blots. To create a simulated western blot dataset, the following was repeated for each condition: 20 cells were selected at random and averaged, until all the cells had been averaged (yielding 30 simulated western blot datapoints per condition). Averaging reduces the size of the dataset to $1/20^{th}$ of the original size, therefore 5 additional conditions containing ICAM2 (see above) were used to create the simulated western blot dataset, for a total of 420 datapoints. For a single cell dataset of equivalent size, 30 cells were selected at random from each of the 14 conditions. This process was repeated 10 times, each with a different random seed, producing 10 different simulated western blot and truncated datasets. The Bayesian network inference procedure (see below) was independently applied to each such dataset.

Bayesian network structure inference. We implemented Bayesian network inference as described in (6, 7) (see also Friedman (8) for a review on the methodology). In the following, we provide a short description of the approach, see the online reference (LINK TO PDF HERE) for more details. Bayesian networks (9) provide a compact graphical representation of multivariate joint probability distributions. This representation consists of a directed acyclic graph whose nodes correspond to random variables, each representing the measured amount of a biomolecule in the dataset. An arc expresses statistical dependence between the downstream variable and the upstream (parent) variable. In certain cases, these statistical dependencies can be interpreted as causal

influences from the parent upon the downstream variable (molecule) (10). For example, Fig. 1C panel b demonstrates how interventional data guides the inference of causality. Once a number of arcs are directed, there are additional arcs whose direction is "compelled", otherwise the resulting graph structure would represent dependencies that do not hold in the data. The Bayesian network associates with each variable X_i, a probability distribution conditioned on its parents in the graph (Pa_i). Intuitively, the values of the parents directly influence the value for X_i. The graph structure represents the dependency assumptions that each variable is independent of its non-descendents, given its parents in the graph; thus the joint distribution can be decomposed into the following product form:

$$P(X_1,\ldots,X_n) = \prod_i P(X_i \mid Pa_i)$$

The goal of Bayesian network inference is to search among possible graphs and select a graph or graphs that best describe the dependency relationships observed in the empirical data. We take a score-based approach: we introduced a statistically motivated scoring function that evaluates each network with respect to the data, and search for the highest scoring network. We use the standard Bayesian scoring metric (11) that rewards relatively simple models (i.e. few arcs), that are likely to have generated the data, that is, whose underlying distribution is close to the empirical distribution of the data. Because our data were sampled under conditions that directly manipulate the amounts of the measured modified biomolecules (see Table 1B), we use an adaptation of the Bayesian scoring metric that explicitly models these interventions (6, 7). Our modeling of interventions assumes that these are *ideal*, i.e. directly affect only one molecule whose

identity is known. While the interventions used are not *ideal*, this is a reasonable first approximation.

Given a scoring function (the Bayesian scoring metric described above) and a set of data, network inference amounts to finding the structure that maximizes the score. The number of possible graph structures is super-exponential in the number of variables (measured biomolecules) and therefore the size of the search space prohibits an exhaustive search. Thus, we resort to a heuristic simulated annealing search. We define a search space where each state is a possible network structure and define a set of operators: addition, deletion or reversal of a single arc, that transform the network from one structure to another. We started with an initial random structure and traversed this space using the operators, searching for high scoring networks. At each step in the search procedure, a random operator was used to change the graph, the resulting structure was rescored and the change was incorporated if it yielded an improvement in the score (To avoid local maxima, occasionally a change was incorporated even if it decreased the score). We iterated this procedure to find high-scoring graphs.

This process was initialized with different random graphs and repeated (500 times), to explore different regions of the search space. Typically, many of the resulting models explained the data almost equally well among themselves. To gain statistical robustness in our inference, instead of relying on a single high scoring structure, we performed model averaging on the compendia of high scoring networks (6). This resulted in an averaged network, consisting of common features (arcs), on which most of the high

scoring network structures agreed. The final inferred network consists of arcs of confidence 85% or greater (that is, appeared in at least 85% of the high scoring networks).

Supplementary Online Materials:

Connection	Influence path	Citation
PKC→Raf	PKC→Ras→Raf$_{S259}$	(12-16)
PKC→Mek	PKC→Raf$_{S497/S499}$→Mek	(17)
PKC→Jnk	PKC→→MKKs→Jnk	(18)
PKC→p38	PKC→→MKKs→p38	(18)
PKC→PKA	PKC →cAMP →PKA	(19)
PKA→Raf	PKA →Raf$_{S259}$	(20)
PKA→Mek	PKA→Raf$_{S621}$→Mek	(21)
PKA→Erk	Unknown	
PKA→Jnk	PKA→→MKKs→Jnk	(22)
PKA→p38	PKA→→MKKs→p38	(23)
Raf→Mek	direct phosphorylation	(24-26)
PKA→Akt	PKA→CaMKK→Akt$_{T308}$→Akt$_{S473}$	(27-29)
Mek→Erk	direct phosphorylation	(30)
Plcγ→PIP2	direct hydrolysis to IP3	(31, 32)
Plcγ→PIP3	recruitment leading to phosphorylation (reversed edge)	(33)
PIP3→PIP2	precursor-product	(33)
Erk→Akt	direct or indirect	(34)

SOM Table 1

Citations for possible pathways of influence listed in Table 1C. The connections and influence paths are as shown in Table 1C (repeated here for convenience).

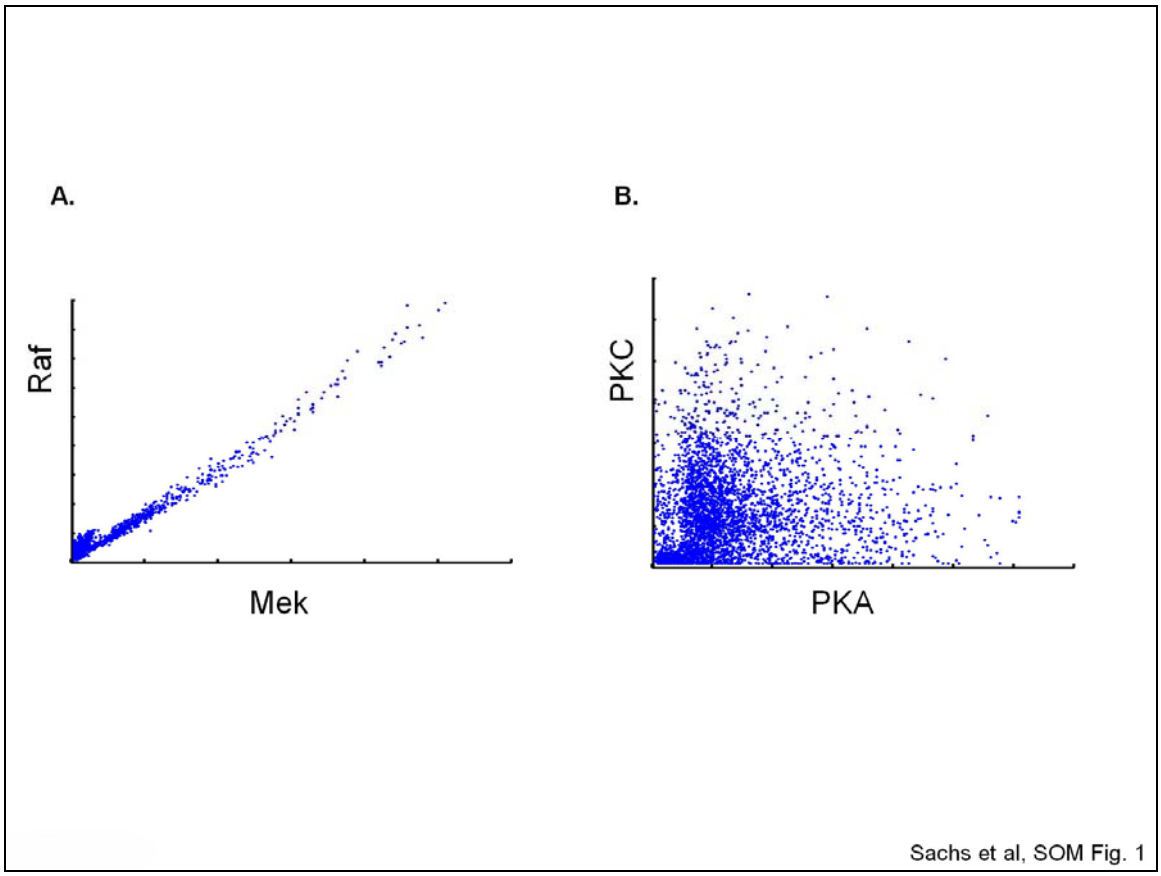

SOM Fig. 1.

Example scatterplots of the multicolor flow cytometry data used. Each dot in the scatter plots represents the amount of two phosphorylated proteins in an individual cell. A. Scatterplot of phosphorylated proteins Raf and Mek shows a clear correlation, similar to the simulated data presented in Fig 1C panel a. B. Scatterplot of PKC and PKA displays a far noisier dependency that is not apparent by eye. The data used contains the entire range between the two examples in this figure. Given sufficient data, the Bayesian network is able to overcome the noise and extract these relationships.

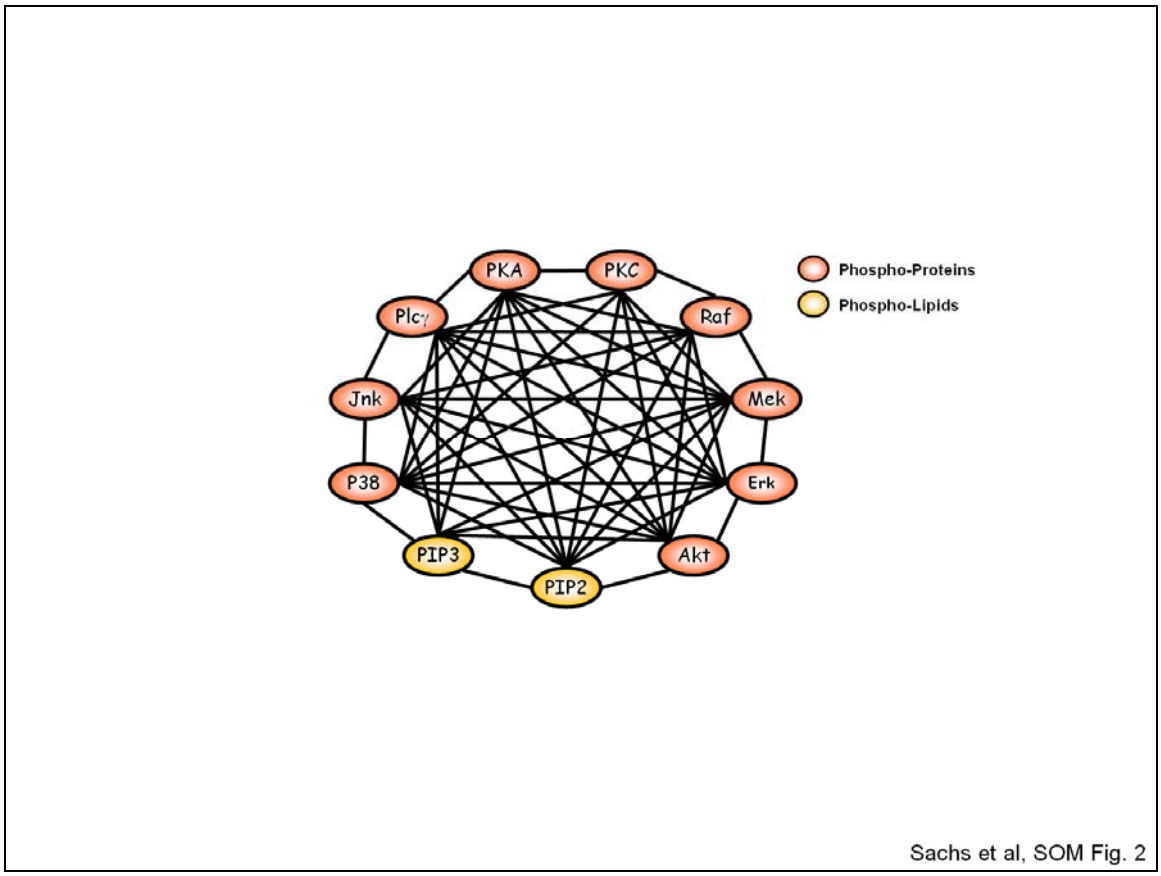

SOM Fig 2.

Correlation connections that pass a Bonferroni corrected p value. 52 out of 55 possible arcs appear. Only the pairs Pip3-Raf, Pip3-PKC and PKC-Jnk are not found to be significantly correlated. Note that correlations are not directed. Thus, there is a need to apply a more rigorous test (Bayesian network inference) to go beyond the simple correlations.

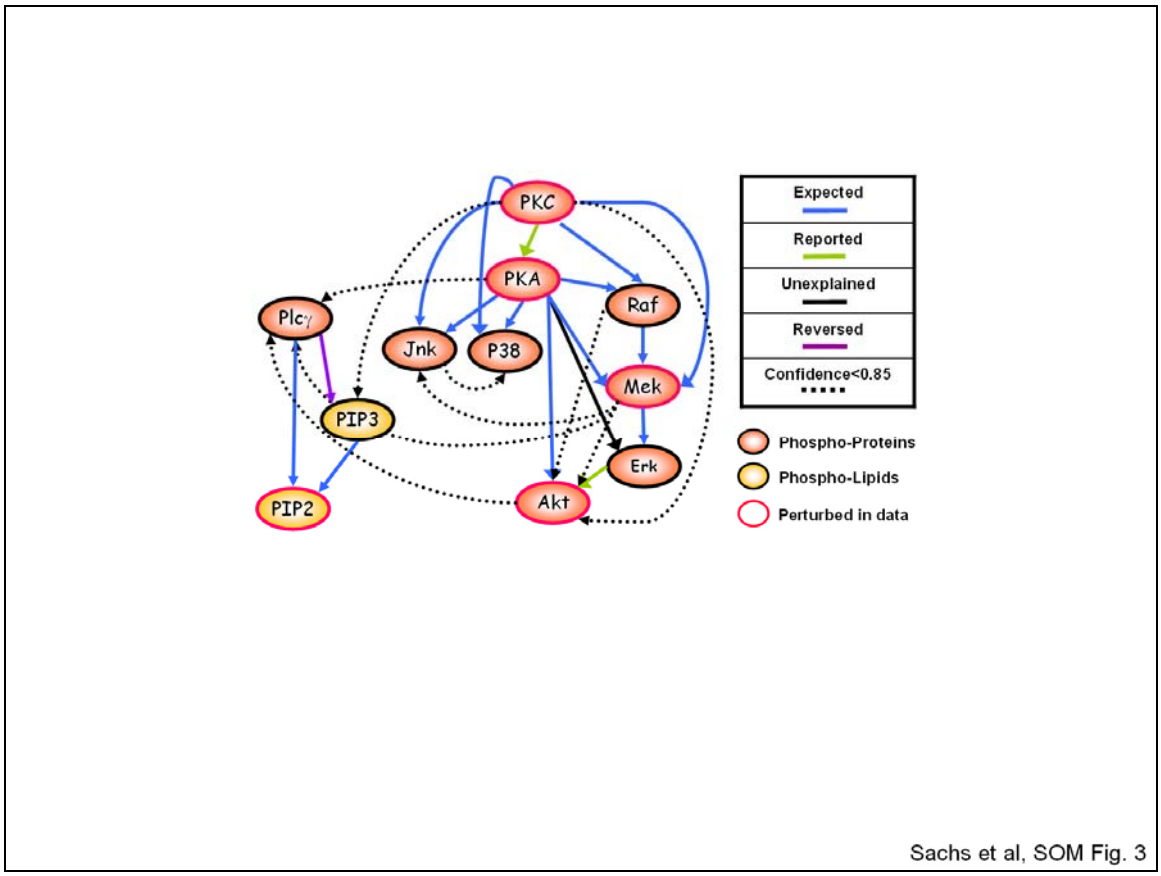

SOM Fig 3.

Inference results including low confidence arcs. Arcs with a confidence value of 0.5 or higher are shown. The lower confidence arcs reveal that each missing arc (from Fig. 3A) is explained by the acyclicity constraint. The missing arc Plcγ→PKC is precluded by the path PKC→PKA→Plcγ, as the addition of the missing Plcγ→PKC arc would form a cycle in the model. Similarly, the arc PIP2→PKC is precluded by the path PKC→PKA→Plcγ→PIP2, and PIP3→Akt is precluded by the path Akt→Plcγ→PIP3. The missing arc Akt→Raf is excluded by the (high confidence) path Raf→Mek→Erk→Akt, but it appears as a low-confidence arc in the reversed (Raf→Akt) direction. Missing arcs clearly demonstrate the limitation in the application of Bayesian network inference to biological pathways due to the acyclicity constraint.

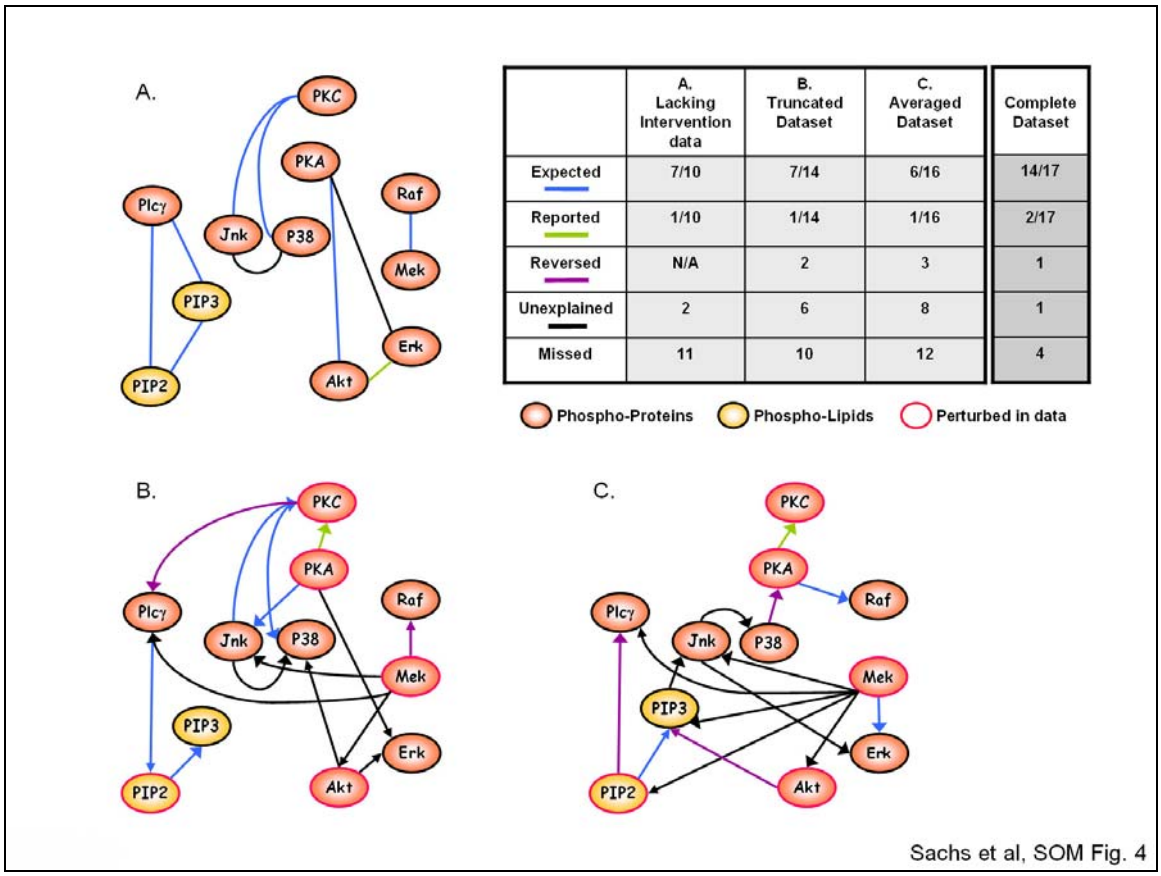

SOM Fig 4. Interventional data, large dataset size and single-cell resolution are critical for effective inference.

A. Inference results from observational data demonstrate that interventional data is crucial for effective inference. Bayesian network analysis was applied to 1200 datapoints from general stimulatory conditions. The resulting network contained only half as many expected arcs and almost three times more missed arcs than the full data counterpart (Fig. 3A). Additionally, while it is sometimes possible to detect directed arcs with observational data alone, in this case no directed arcs were found, so the model provides no information regarding the causal direction of each link.

B. Results from a truncated version of the full dataset reveal the importance of very large dataset size. Although this dataset contains all the interventions as in the full dataset, its

smaller size (420 datapoints) resulted in fewer expected connections recovered and more missing arcs as compared to the result from the full dataset (Fig.3A).

C. Results from averaged, simulated western blot data indicate the advantage of single-cell resolution. Simulated western blot data was created by averaging 20 randomly selected single-cell data points at a time, yielding a dataset of 420 points. As compared to a single-cell dataset of equal size (SOM Fig. 4B), this result missed more arcs and captures more unconfirmed arcs. Ten sets of truncated and averaged datasets were made; results shown in B and C represent typical results.

Supplementary References.

1. Perez, O. D., Krutzik, P. O. & Nolan, G. P. (2004) *Methods Mol Biol* **263,** 67-94.
2. Perez, O. D. & Nolan, G. P. (2002) *Nat Biotechnol* **20,** 155-62.
3. Tung, J. W., Parks, D. R., Moore, W. A. & Herzenberg, L. A. (2004) *Methods Mol Biol* **271,** 37-58.
4. Lenz, P., Bacot, S. M., Frazier-Jessen, M. R. & Feldman, G. M. (2003) *FEBS Lett* **538,** 149-54.
5. Hartemink, A. J. & Massachusetts Institute of Technology. Dept. of Electrical Engineering and Computer Science. (2001), pp. 206 p.
6. Pe'er, D., Regev, A., Elidan, G. & Friedman, N. (2001) *Bioinformatics* **17 Suppl 1,** S215-24.
7. Yoo, C. a. C. G. F. (1999) in *Uncertainty in Artificial Intelligence*, pp. 116-125.
8. Friedman, N. (2004) *Science* **303,** 799-805.
9. Pearl, J. (1988) *Probabilistic reasoning in intelligent systems : networks of plausible inference* (Morgan Kaufmann Publishers, San Mateo, Calif.).
10. Pearl, J. (2000) *Causality : Models, Reasoning, and Inference* (Cambridge University Press.
11. Heckerman, D. (1995) in *Microsoft Research*, Vol. MSR-TR-95-06.
12. Van Aelst, L., Barr, M., Marcus, S., Polverino, A. & Wigler, M. (1993) *Proc Natl Acad Sci U S A* **90,** 6213-7.
13. Marais, R., Light, Y., Mason, C., Paterson, H., Olson, M. F. & Marshall, C. J. (1998) *Science* **280,** 109-12.
14. Marais, R., Light, Y., Paterson, H. F. & Marshall, C. J. (1995) *Embo J* **14,** 3136-45.
15. Jaumot, M. & Hancock, J. F. (2001) *Oncogene* **20,** 3949-58.
16. Marshall, C. J. (1994) *Curr Opin Genet Dev* **4,** 82-9.
17. Carroll, M. P. & May, W. S. (1994) *J Biol Chem* **269,** 1249-56.
18. Clerk, A., Pham, F. H., Fuller, S. J., Sahai, E., Aktories, K., Marais, R., Marshall, C. & Sugden, P. H. (2001) *Mol Cell Biol* **21,** 1173-84.
19. Zhang, W. M. & Wong, T. M. (1998) *Am J Physiol* **274,** C82-7.
20. Dhillon, A. S., Pollock, C., Steen, H., Shaw, P. E., Mischak, H. & Kolch, W. (2002) *Mol Cell Biol* **22,** 3237-46.
21. Mischak, H., Seitz, T., Janosch, P., Eulitz, M., Steen, H., Schellerer, M., Philipp, A. & Kolch, W. (1996) *Mol Cell Biol* **16,** 5409-18.
22. Fortino, V., Torricelli, C., Gardi, C., Valacchi, G., Rossi Paccani, S. & Maioli, E. (2002) *Cell Mol Life Sci* **59,** 2165-71.
23. Zheng, M., Zhang, S. J., Zhu, W. Z., Ziman, B., Kobilka, B. K. & Xiao, R. P. (2000) *J Biol Chem* **275,** 40635-40.
24. Lange-Carter, C. A. & Johnson, G. L. (1994) *Science* **265,** 1458-61.
25. Jaiswal, R. K., Moodie, S. A., Wolfman, A. & Landreth, G. E. (1994) *Mol Cell Biol* **14,** 6944-53.
26. Vaillancourt, R. R., Gardner, A. M. & Johnson, G. L. (1994) *Mol Cell Biol* **14,** 6522-30.
27. Wayman GA, T. H., Soderling TR. (1997) *J Biol Chem* **26,** 16073-6.
28. Yano, S., Tokumitsu, H., and Soderling, T.R. (1998) *Nature***,** 584-587.

29. Toker A, N. A. (2000) *J Biol Chem* **12,** 8271-4.
30. Payne, D. M., Rossomando, A. J., Martino, P., Erickson, A. K., Her, J. H., Shabanowitz, J., Hunt, D. F., Weber, M. J. & Sturgill, T. W. (1991) *Embo J* **10,** 885-92.
31. Sofroniew, M. V., Howe, C. L. & Mobley, W. C. (2001) *Annu Rev Neurosci* **24,** 1217-81.
32. Lee, S. B. & Rhee, S. G. (1995) *Curr Opin Cell Biol* **7,** 183-9.
33. Alberts, B. (2002) *Molecular biology of the cell* (Garland Science, New York).
34. Fukuda, R., Kelly, B. & Semenza, G. L. (2003) *Cancer Res* **63,** 2330-4.